
DILATED CONVOLUTION WITH LEARNABLE SPACINGS

*Ismail Khalfaoui-Hassani^{1,6}, Thomas Pellegrini^{1,3,4,5,6}, and Timothée Masquelier^{2,4,6}

¹Artificial and Natural Intelligence Toulouse Institute (ANITI), ²CerCo UMR 5549, ³IRIT, ⁴CNRS, ⁵Toulouse INP, UT3, ⁶Université de Toulouse, France

ABSTRACT

Recent works indicate that convolutional neural networks (CNN) need large receptive fields (RF) to compete with visual transformers and their attention mechanism. In CNNs, RFs can simply be enlarged by increasing the convolution kernel sizes. Yet the number of trainable parameters, which scales quadratically with the kernel’s size in the 2D case, rapidly becomes prohibitive, and the training is notoriously difficult. This paper presents a new method to increase the RF size without increasing the number of parameters. The dilated convolution (DC) has already been proposed for the same purpose. DC can be seen as a convolution with a kernel that contains only a few non-zero elements placed on a regular grid. Here we present a new version of the DC in which the spacings between the non-zero elements, or equivalently their positions, are no longer fixed but learnable via backpropagation thanks to an interpolation technique. We call this method “Dilated Convolution with Learnable Spacings” (DCLS) and generalize it to the n-dimensional convolution case. However, our main focus here will be on the 2D case. We first tried our approach on ResNet50: we drop-in replaced the standard convolutions with DCLS ones, which increased the accuracy of ImageNet1k classification at iso-parameters, but at the expense of the throughput. Next, we used the recent ConvNeXt state-of-the-art convolutional architecture and drop-in replaced the depthwise convolutions with DCLS ones. This not only increased the accuracy of ImageNet1k classification but also of typical downstream and robustness tasks, again at iso-parameters but this time with negligible cost on throughput, as ConvNeXt uses separable convolutions. Conversely, classic DC led to poor performance with both ResNet50 and ConvNeXt. The code of the method is based on Pytorch and available.¹

1 INTRODUCTION

The receptive field of a deep convolutional network is a crucial element to take into account when dealing with recognition and downstream tasks in computer vision. For instance, a logarithmic relationship between classification accuracy and receptive field size was observed in Araujo et al. (2019). This tells us that large receptive fields are necessary for high-level vision tasks, but with logarithmically decreasing rewards and thus a higher computational cost to reach them.

Recent advances in vision transformers (Dosovitskiy et al., 2020) and in CNNs (Liu et al., 2022b; Ding et al., 2022; Trockman & Kolter, 2022; Liu et al., 2022a) highlight the beneficial effect that a large convolution kernel can have, compared to the 3×3 kernels traditionally used in previous state-of-the-art CNN models (He et al., 2016). However, when naively increasing the kernel size, the accuracy rapidly plateaus or even decreases. For example, in ConvNeXt, the best accuracy was achieved by a 7×7 kernel (Liu et al., 2022b;a). Using a structural re-parameterization trick, Ding et al. (2022) demonstrated the benefit of increasing the kernel size up to 31 by 31. Thereafter, Liu et al. (2022a) showed that there was still room for improvement by moving to 51 by 51, using the *depthwise implicit matrix multiplication (gemm)* method developed by Ding et al. (2022), in addition to a spatial separation of the depthwise kernel followed by an accumulation of the resulting

*Corresponding Author: ismail.khalifaoui-hassani@univ-tlse3.fr

¹<https://github.com/K-H-Ismail/Dilated-Convolution-with-Learnable-Spacings-PyTorch>

activations. Yet, all these improvements have a cost in terms of memory and computation and it does not seem possible to increase the size of the kernels indefinitely.

One of the first approaches that allows inflating the receptive field of a convolutional layer without increasing the number of learnable parameters nor the computational cost is called dilated convolution (DC). DC or “atrous convolution” was first described in Holschneider et al. (1990) and Shensa (1992), under the name “convolution with a dilated filter” before being referred to as “dilated convolution” in Yu & Koltun (2015). The purpose of this approach is to inflate the convolutional kernel by regularly inserting spaces (*i.e.* zeros) between the kernel elements, as depicted in Figure 2b. The spacing between elements is thus constant, it is a hyper-parameter usually referred to as “dilation” or “dilation rate”. Despite its early successes in classification since Yu et al. (2017), and its even

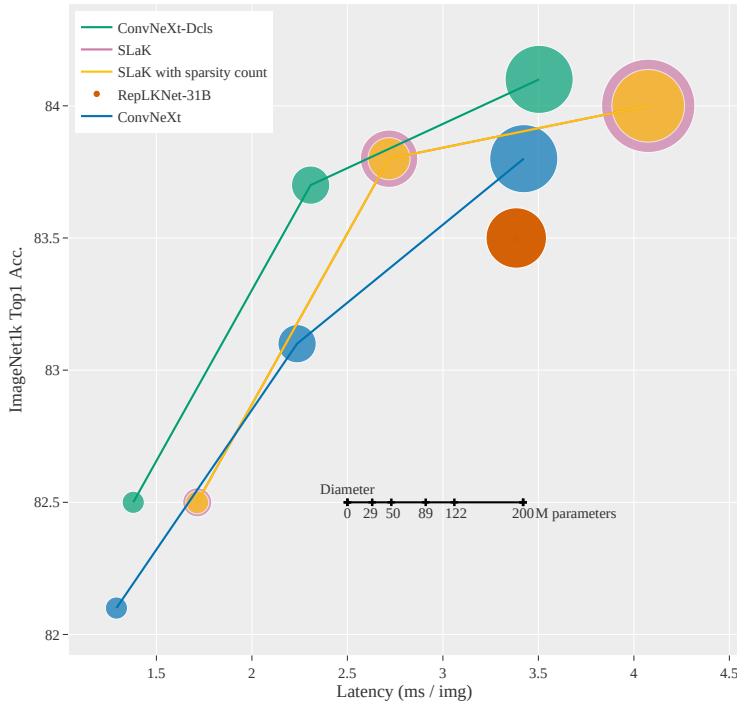


Figure 1: Classification accuracy on ImageNet-1K as a function of latency. Dot diameter corresponds to the number of parameters.

more convincing results in semantic segmentation Sandler et al. (2018); Chen et al. (2017; 2018) and object detection Lu et al. (2019), DC has gradually fallen out of favor and has been confined to downstream tasks such as those described above. Without much success, Ding et al. (2022) tried to implement DC in their ReplKNet architecture. Our own investigation on ResNet and ConvNeXt with standard dilated convolution (Section 4.2) will lead to a similar conclusion. The failure of this method for classification tasks could be attributed to the great rigidity imposed by its regular grid as discussed in Wang & Ji (2018).

In this context, we propose DCLS (Dilated Convolution with Learnable Spacings), a new convolution method. In DCLS, the positions of the non-zero elements within the convolutional kernels are learned in a gradient-based manner. The inherent problem of non-differentiability due to the integer nature of the positions in the kernel is circumvented by interpolation (Fig. 2c). DCLS is a differentiable method that only constructs the convolutional kernel. To actually apply the method, we could either use the native convolution provided by Pytorch or a more advanced one such as the *depthwise implicit gemm* convolution method (Ding et al., 2022), using the constructed kernel. DCLS comes in six sub-versions: 1D, 2D, 3D and what we call N-MD methods, namely: “2-1D, 3-1D and 3-2D” where a N-dimension kernel is used but positions are learned only along M dimension(s). The main focus of this paper will be the 2D version for which we detail mathematical proofs, implementation specificities and results on image classification, downstream and robustness tasks.

Instead of having a grid of kernel elements like in standard and dilated convolutions, DCLS allows an arbitrary number of kernel elements (Fig. 2d). We refer to this free tunable hyper-parameter as “kernel count”. In this paper we set it in order to be at iso or fewer parameters than the baselines we will compare ourselves to. Conversely, we refer to the size of the kernel, or rather the maximum size in which the kernel elements are allowed to move inside the dilated kernel, as the “dilated kernel size”. It is also a tunable hyper-parameter.

The positions of kernel elements in DCLS are randomly initialized, and are allowed to move throughout the learning process within the dilated kernel size limit. We will then show how sharing positions across multiple blocks of a same convolution stage could further increase accuracy while reducing the number of learnable parameters. This, together with other learning techniques, empirically and consistently improve the overall performance of the method. They are summarized in Section 3.

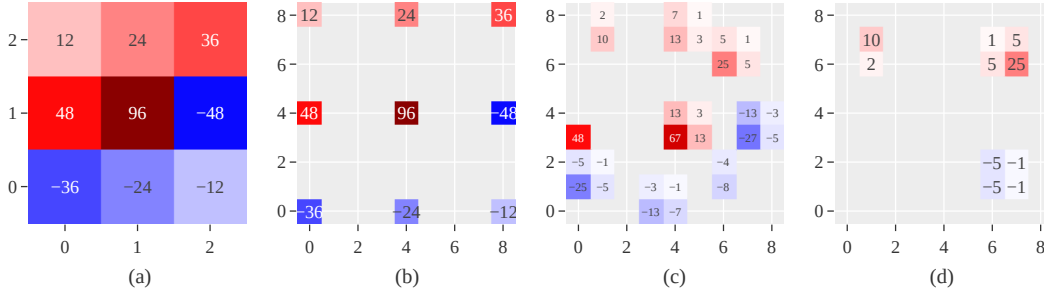


Figure 2: (a): a standard 3×3 kernel. (b): a dilated 3×3 kernel with dilation rate 4. (c): a DCLS2d kernel with 9 kernel elements and a dilated kernel size of 9. Each weight is spread over up to four adjacent pixels. (d): a DCLS2d kernel with 3 kernel elements and still a dilated kernel size of 9.

2 KERNEL CONSTRUCTION IN DCLS

In the following, we show how to mathematically describe the DCLS kernel construction and how to explicitly calculate the gradients of the loss function with respect to weights and positions that are used in the backpropagation algorithm. These gradients are useful to implement the DCLS method in a way that is compatible with the automatic differentiation of Pytorch.

2.1 NOTATION AND PRELIMINARIES

We denote by $\lfloor \cdot \rfloor$ the floor function and we define its derivative by the zero function.

$$\forall x \in \mathbb{R}, \lfloor x \rfloor' \stackrel{\text{def}}{=} 0 \quad (1)$$

We denote by $m \in \mathbb{N}^*$ the number of kernel elements inside the constructed kernel and we refer to it as the “kernel count”. Moreover, we denote respectively by $s_1, s_2 \in \mathbb{N}^* \times \mathbb{N}^*$, the sizes of the constructed kernel along the x-axis and the y-axis. The latter could be seen as the limits of the dilated kernel, and we refer to them as the “dilated kernel size”.

The $n \times p$ matrix space over \mathbb{R} is defined as the set of all $n \times p$ matrices over \mathbb{R} , and is denoted $\mathcal{M}_{n,p}(\mathbb{R})$.

The Frobenius inner product \times_F of two matrices A and B of $\mathcal{M}_{n,p}(\mathbb{R})$ is defined by:

$$A \times_F B = \text{tr}(A^T B)$$

Where “tr” stands for the trace of the square matrix $A^T B$.

The characters w , p^1 and p^2 respectively stand for the weight, the position of that weight along the x-axis (width) and its position along the y-axis (height) in the scalar case while the bold $w =$

$(w_i)_{1 \leq i \leq m}$, $\mathbf{p}^1 = (p_i^1)_{1 \leq i \leq m}$ and $\mathbf{p}^2 = (p_i^2)_{1 \leq i \leq m}$ respectively stand for the weight, the width-position of that weight and its height-position in the vector case.

The proofs and algorithms that will be shown in the next sections are made for the case of tensors with one input channel and one output channel. Without loss of generality, those proofs and algorithms hold for the general case of 4D tensors and higher by considering and applying them channel-wise.

2.2 2D-DCLS, SCALAR WEIGHT CASE

We begin by the case of a kernel containing only one element.

The function f that defines the kernel construction in the scalar weight case is as follows:

$$\begin{aligned} f: \mathbb{R} \times \mathbb{R} \times \mathbb{R} &\rightarrow \mathcal{M}_{s_1, s_2}(\mathbb{R}) \\ w, p^1, p^2 &\mapsto \mathbf{K} \end{aligned} \quad (2)$$

where $\forall i \in [1 \dots s_1], \forall j \in [1 \dots s_2]$:

$$\mathbf{K}_{ij} = \begin{cases} w(1-r^1)(1-r^2) & \text{if } i = \lfloor p^1 \rfloor, j = \lfloor p^2 \rfloor \\ w r^1 (1-r^2) & \text{if } i = \lfloor p^1 \rfloor + 1, j = \lfloor p^2 \rfloor \\ w(1-r^1)r^2 & \text{if } i = \lfloor p^1 \rfloor, j = \lfloor p^2 \rfloor + 1 \\ w r^1 r^2 & \text{if } i = \lfloor p^1 \rfloor + 1, j = \lfloor p^2 \rfloor + 1 \\ 0 & \text{otherwise} \end{cases} \quad (3)$$

and where the fractional parts are:

$$r^1 = \{p^1\} = p^1 - \lfloor p^1 \rfloor \quad \text{and} \quad r^2 = \{p^2\} = p^2 - \lfloor p^2 \rfloor \quad (4)$$

The constructed kernel \mathbf{K} is zero except for at most the 4 adjacent positions that represent the 2D interpolation of the single weight w . Note that $\sum_{j=1}^{s_2} \sum_{i=1}^{s_1} \mathbf{K}_{ij} = w$. We then define the scalar loss function as

$$loss = g(f(w, p^1, p^2)) \quad (5)$$

with $g: \mathcal{M}_{s_1, s_2}(\mathbb{R}) \rightarrow \mathbb{R}$ a differentiable function that models the action of all the layers that will follow f in the model.

By applying the chain rule we obtain

$$\frac{\partial loss}{\partial w} = g'(f(w, p^1, p^2)) \times_{\mathbb{F}} \frac{\partial f(w, p^1, p^2)}{\partial w} \quad (6)$$

$$\frac{\partial loss}{\partial p^1} = g'(f(w, p^1, p^2)) \times_{\mathbb{F}} \frac{\partial f(w, p^1, p^2)}{\partial p^1} \quad (7)$$

$$\frac{\partial loss}{\partial p^2} = g'(f(w, p^1, p^2)) \times_{\mathbb{F}} \frac{\partial f(w, p^1, p^2)}{\partial p^2} \quad (8)$$

with

$$g'(f(w, p^1, p^2)) = \frac{\partial loss}{\partial \mathbf{K}} = \frac{\partial loss}{\partial f(w, p^1, p^2)} \quad (9)$$

Let us put

$$g'(f(w, p^1, p^2)) = \mathbf{G} = \begin{bmatrix} g_{11} & g_{12} & \cdots & g_{1s_2} \\ g_{21} & \ddots & & g_{2s_2} \\ \vdots & & \ddots & \vdots \\ g_{s_1 1} & g_{s_1 2} & \cdots & g_{s_1 s_2} \end{bmatrix} \quad (10)$$

We show that the gradients of the loss function with respect to weights and positions in scalar weight case is (details of the proof are in Appendix A):

$$\begin{aligned} \frac{\partial loss}{\partial w} &= (1 - r^1) (1 - r^2) g_{\lfloor p^1 \rfloor \lfloor p^2 \rfloor} + r^1 (1 - r^2) g_{\lfloor p^1 \rfloor + 1 \lfloor p^2 \rfloor} \\ &\quad + (1 - r^1) r^2 g_{\lfloor p^1 \rfloor \lfloor p^2 \rfloor + 1} + r^1 r^2 g_{\lfloor p^1 \rfloor + 1 \lfloor p^2 \rfloor + 1} \end{aligned} \quad (11)$$

$$\begin{aligned} \frac{\partial loss}{\partial p^1} &= w [-(1 - r^2) g_{\lfloor p^1 \rfloor \lfloor p^2 \rfloor} + (1 - r^2) g_{\lfloor p^1 \rfloor + 1 \lfloor p^2 \rfloor} \\ &\quad - r^2 g_{\lfloor p^1 \rfloor \lfloor p^2 \rfloor + 1} + r^2 g_{\lfloor p^1 \rfloor + 1 \lfloor p^2 \rfloor + 1}] \end{aligned} \quad (12)$$

$$\begin{aligned} \frac{\partial loss}{\partial p^2} &= w [-(1 - r^1) g_{\lfloor p^1 \rfloor \lfloor p^2 \rfloor} - r^1 g_{\lfloor p^1 \rfloor + 1 \lfloor p^2 \rfloor} \\ &\quad + (1 - r^1) g_{\lfloor p^1 \rfloor \lfloor p^2 \rfloor + 1} + r^1 g_{\lfloor p^1 \rfloor + 1 \lfloor p^2 \rfloor + 1}] \end{aligned} \quad (13)$$

2.3 2D-DCLS, GENERAL CASE

The general case is the one where the weights $\mathbf{w} = [w_1 \ w_2 \ \dots \ w_m]^T$ and the positions $\mathbf{p}^1 = [p_1^1 \ p_2^1 \ \dots \ p_m^1]^T$, $\mathbf{p}^2 = [p_1^2 \ p_2^2 \ \dots \ p_m^2]^T$ are stored in vectors, with the fractional parts $\mathbf{r}^1 = \{\mathbf{p}^1\} = \mathbf{p}^1 - \lfloor \mathbf{p}^1 \rfloor = [r_1^1 \ r_2^1 \ \dots \ r_m^1]^T$ and $\mathbf{r}^2 = \{\mathbf{p}^2\} = \mathbf{p}^2 - \lfloor \mathbf{p}^2 \rfloor = [r_1^2 \ r_2^2 \ \dots \ r_m^2]^T$ extended as well.

The function f defined in equation (2) is then extended to the function F defined as follows:

$$\begin{aligned} F: \mathbb{R}^m \times \mathbb{R}^m \times \mathbb{R}^m &\rightarrow \mathcal{M}_{s_1, s_2}(\mathbb{R}) \\ \mathbf{w}, \mathbf{p}^1, \mathbf{p}^2 &\mapsto \mathbf{K} = \sum_{i=1}^m f(w_i, p_i^1, p_i^2) \end{aligned} \quad (14)$$

The constructed kernel \mathbf{K} here is the result of a summation of the function f defined in (2) over the elements of weight and position vectors. We then define the scalar loss function as in (5).

$$loss = g(F(\mathbf{w}, \mathbf{p}^1, \mathbf{p}^2)) \quad (15)$$

with $g: \mathcal{M}_{s_1, s_2}(\mathbb{R}) \rightarrow \mathbb{R}$ a differentiable function that models the action of all the layers that will follow F in the model.

Let us put

$$g'(F(\mathbf{w}, \mathbf{p}^1, \mathbf{p}^2)) = \mathbf{G} = \begin{bmatrix} g_{11} & g_{12} & \dots & g_{1s_2} \\ g_{21} & \ddots & & g_{2s_2} \\ \vdots & & \ddots & \vdots \\ g_{s_1 1} & g_{s_1 2} & \dots & g_{s_1 s_2} \end{bmatrix} \quad (16)$$

We show that the gradients of the loss function with respect to weights and positions in the general case (details of the proof are in Appendix B):

$\forall i \in \llbracket 1 \dots m \rrbracket$:

$$\begin{aligned} \left(\frac{\partial loss}{\partial w} \right)_i &= (1 - r_i^1) (1 - r_i^2) g_{\lfloor p_i^1 \rfloor \lfloor p_i^2 \rfloor} + r_i^1 (1 - r_i^2) g_{\lfloor p_i^1 \rfloor + 1 \lfloor p_i^2 \rfloor} \\ &\quad + (1 - r_i^1) r_i^2 g_{\lfloor p_i^1 \rfloor \lfloor p_i^2 \rfloor + 1} + r_i^1 r_i^2 g_{\lfloor p_i^1 \rfloor + 1 \lfloor p_i^2 \rfloor + 1} \end{aligned} \quad (17)$$

$$\begin{aligned} \left(\frac{\partial loss}{\partial p^1} \right)_i &= w_i [-(1 - r_i^2) g_{\lfloor p_i^1 \rfloor \lfloor p_i^2 \rfloor} + (1 - r_i^2) g_{\lfloor p_i^1 \rfloor + 1 \lfloor p_i^2 \rfloor} \\ &\quad - r_i^2 g_{\lfloor p_i^1 \rfloor \lfloor p_i^2 \rfloor + 1} + r_i^2 g_{\lfloor p_i^1 \rfloor + 1 \lfloor p_i^2 \rfloor + 1}] \end{aligned} \quad (18)$$

$$\begin{aligned} \left(\frac{\partial loss}{\partial p^2} \right)_i &= w_i [-(1 - r_i^1) g_{\lfloor p_i^1 \rfloor \lfloor p_i^2 \rfloor} - r_i^1 g_{\lfloor p_i^1 \rfloor + 1 \lfloor p_i^2 \rfloor} \\ &\quad + (1 - r_i^1) g_{\lfloor p_i^1 \rfloor \lfloor p_i^2 \rfloor + 1} + r_i^1 g_{\lfloor p_i^1 \rfloor + 1 \lfloor p_i^2 \rfloor + 1}] \end{aligned} \quad (19)$$

Remark: The extension to the 1D and 3D convolution cases is provided in Appendix C.

2.4 FORWARD AND BACKWARD ALGORITHMS FOR 2D-DCLS KERNEL CONSTRUCTION

The derivations obtained above allow us to develop the 2D-DCLS kernel construction algorithm. In the following, we describe with pseudocode the forward and backward passes for kernel construction used in 2D-DCLS. In practice, \mathbf{W} , \mathbf{P}^1 and \mathbf{P}^2 are 3-D tensors of size (channels_out, channels_in // groups, K_count), but the algorithms presented here are easily extended to this case by applying them channel-wise.

Algorithm 1 2D-DCLS kernel construction forward pass

Input: \mathbf{W} , \mathbf{P}^1 , \mathbf{P}^2 : vectors of dimension m

Output: \mathbf{K} : the constructed kernel, of size ($s_1 \times s_2$)

```

1:  $\mathbf{K} \leftarrow 0$ 
2:  $\mathbf{p}^1 \leftarrow \lfloor \mathbf{P}^1 \rfloor$ ;  $\mathbf{p}^2 \leftarrow \lfloor \mathbf{P}^2 \rfloor$ 
3:  $\mathbf{R}^1 \leftarrow \mathbf{P}^1 - \mathbf{p}^1$ ;  $\mathbf{R}^2 \leftarrow \mathbf{P}^2 - \mathbf{p}^2$ 
4: save_for_backward ( $\mathbf{p}^1, \mathbf{p}^2, \mathbf{R}^1, \mathbf{R}^2$ )
5: for  $i = 0 \rightarrow m - 1$  do
6:    $\mathbf{K}[\mathbf{p}_i^1, \mathbf{p}_i^2] += \mathbf{W}_i * (1 - \mathbf{R}_i^1) * (1 - \mathbf{R}_i^2)$ 
7:    $\mathbf{K}[\mathbf{p}_i^1 + 1, \mathbf{p}_i^2] += \mathbf{W}_i * (\mathbf{R}_i^1) * (1 - \mathbf{R}_i^2)$ 
8:    $\mathbf{K}[\mathbf{p}_i^1, \mathbf{p}_i^2 + 1] += \mathbf{W}_i * (1 - \mathbf{R}_i^1) * (\mathbf{R}_i^2)$ 
9:    $\mathbf{K}[\mathbf{p}_i^1 + 1, \mathbf{p}_i^2 + 1] += \mathbf{W}_i * (\mathbf{R}_i^1) * (\mathbf{R}_i^2)$ 
10: end for

```

Algorithm 2 2D-DCLS kernel construction backward pass

Input: $\text{GradK} = \frac{\partial \text{Loss}}{\partial \mathbf{K}}$: matrix of dimension ($s_1 \times s_2$)

Output: $\frac{\partial \text{Loss}}{\partial \mathbf{W}}$, $\frac{\partial \text{Loss}}{\partial \mathbf{P}^1}$, $\frac{\partial \text{Loss}}{\partial \mathbf{P}^2}$: vectors of dimension m

```

1:  $\frac{\partial \text{Loss}}{\partial \mathbf{W}} \leftarrow 0$ ,  $\frac{\partial \text{Loss}}{\partial \mathbf{P}^1} \leftarrow 0$ ,  $\frac{\partial \text{Loss}}{\partial \mathbf{P}^2} \leftarrow 0$ 
2:  $\mathbf{p}^1, \mathbf{p}^2, \mathbf{R}^1, \mathbf{R}^2 \leftarrow \text{load\_saved} ( )$ 
3: for  $i = 0 \rightarrow m - 1$  do
4:

```

$$\begin{aligned} \frac{\partial \text{Loss}}{\partial \mathbf{W}} [i] += & \frac{\partial \text{Loss}}{\partial \mathbf{K}} [\mathbf{p}_i^1, \mathbf{p}_i^2] * (1 - \mathbf{R}_i^1) * (1 - \mathbf{R}_i^2) + \frac{\partial \text{Loss}}{\partial \mathbf{K}} [\mathbf{p}_i^1 + 1, \mathbf{p}_i^2] * \mathbf{R}_i^1 * (1 - \mathbf{R}_i^2) \\ & + \frac{\partial \text{Loss}}{\partial \mathbf{K}} [\mathbf{p}_i^1, \mathbf{p}_i^2 + 1] * (1 - \mathbf{R}_i^1) * \mathbf{R}_i^2 + \frac{\partial \text{Loss}}{\partial \mathbf{K}} [\mathbf{p}_i^1 + 1, \mathbf{p}_i^2 + 1] * \mathbf{R}_i^1 * \mathbf{R}_i^2 \end{aligned}$$

5:

$$\begin{aligned} \frac{\partial \text{Loss}}{\partial \mathbf{P}^1} [i] += & \mathbf{W}_i * \left[-\frac{\partial \text{Loss}}{\partial \mathbf{K}} [\mathbf{p}_i^1, \mathbf{p}_i^2] * (1 - \mathbf{R}_i^2) + \frac{\partial \text{Loss}}{\partial \mathbf{K}} [\mathbf{p}_i^1 + 1, \mathbf{p}_i^2] * (1 - \mathbf{R}_i^2) \right. \\ & \left. - \frac{\partial \text{Loss}}{\partial \mathbf{K}} [\mathbf{p}_i^1, \mathbf{p}_i^2 + 1] * \mathbf{R}_i^2 + \frac{\partial \text{Loss}}{\partial \mathbf{K}} [\mathbf{p}_i^1 + 1, \mathbf{p}_i^2 + 1] * \mathbf{R}_i^2 \right] \end{aligned}$$

6:

$$\begin{aligned} \frac{\partial \text{Loss}}{\partial \mathbf{P}^2} [i] += & \mathbf{W}_i * \left[-\frac{\partial \text{Loss}}{\partial \mathbf{K}} [\mathbf{p}_i^1, \mathbf{p}_i^2] * (1 - \mathbf{R}_i^1) - \frac{\partial \text{Loss}}{\partial \mathbf{K}} [\mathbf{p}_i^1 + 1, \mathbf{p}_i^2] * \mathbf{R}_i^1 \right. \\ & \left. + \frac{\partial \text{Loss}}{\partial \mathbf{K}} [\mathbf{p}_i^1, \mathbf{p}_i^2 + 1] * (1 - \mathbf{R}_i^1) + \frac{\partial \text{Loss}}{\partial \mathbf{K}} [\mathbf{p}_i^1 + 1, \mathbf{p}_i^2 + 1] * \mathbf{R}_i^1 \right] \end{aligned}$$

7: end for

The nested for loop in the algorithms is fully parallelized using GPU threads. The 2D-DCLS convolution with kernel construction is then obtained by applying the classical 2D-convolution provided natively by Pytorch or any other method such as the *depthwise implicit gemm* convolution method Ding et al. (2022) using the constructed kernel.

3 LEARNING TECHNIQUES

So far we have seen how to implement the DCLS method. We now turn to the techniques that allow us to get the most out of the method. In what follows, we list the training techniques that we have retained and for which we have noticed a consistent and empirical advantage on validation accuracy.

- **Weight decay:** weight decay is a regularization method widely used in a variety of deep learning models. Though its beneficial effect on generalization, we noticed that when applied to the kernel positions parameters in DCLS method, this last tend to "artificially" over-concentrate the positions around the center of the kernel, resulting in poorer accuracy. Therefore, we set this hyperparameter to 0 for the kernel positions parameters and kept it unchanged for all the other parameters.
- **Positions initialization:** the DCLS positions tend to cluster around the center of the RF throughout the learning process (see Appendix D). In an attempt to facilitate learning, we chose an initial distribution close to the one obtained at the end of training, that is a centered normal law of standard deviation 0.5. Yet in practice the uniform law gives similar performance.
- **Positions Clamping:** kernel elements that reach the dilated kernel size limit are clamped. This is done at the end of every batch step to force kernel positions to stay within the limits. Agglutination around those limits can sometimes be observed and this indicates that the dilated kernel size is too small and should be enlarged. Positions of different kernel weights (or their interpolations) could also overlap. They are added together in such case.
- **Dilated kernel size tuning:** we empirically tuned it using the remark said above. Note that increasing the dilated kernel size has no cost on the number of trainable parameters, but has a cost on throughput, especially when using non-separable convolutions. For simplicity, we used the same dilated kernel size in all the model layers (7 for ResNet-50-dcls and 17 for ConvNeXt-dcls).
- **Kernel count tuning:** as said before, we have set this hyper-parameter to the maximal integer value that allows us to be below the baselines to which we compare ourselves in terms of the number of trainable parameters. Note that adding one element to the 2D-DCLS kernel leads to having three additional learnable parameters: the weight, its vertical and its horizontal position. For simplicity, we used the same kernel count in all the model layers.
- **Positions learning rate scaling:** we found that kernel positions could benefit from a special scaling when it comes to the learning rate. As their magnitude is different from regular weights, we scaled the learning rate of all the kernel positions parameters by a factor of 5. This is the best factor we found empirically. Custom-made schedulers for positions have been tested, but scaling the learning rate while using the same scheduler as for the kernel weights remained the best choice. Interestingly, we found that throughout learning, the average speed of the positions follows precisely the shape of the learning rate scheduler curve (Appendix E).
- **Synchronizing positions:** we shared the kernel positions across convolution layers that have the same number of parameters (typically, those belonging to a same stage of the ConvNeXt/ResNet model), without sharing the weights. Positions in these kind of stages were centralized in common parameters that accumulate the gradients. This constraint has surprisingly enhanced the accuracy, while reducing the number of extra parameters dedicated to positions.
- **Repulsive loss:** following the work of Thomas et al. (2019) on 3D cloud points, we implemented the repulsive loss for the DCLS kernel positions, in order to discourage multiple elements from overlapping. Despite a slight advantage with the ResNet-50 model, this technique did not significantly improve the results with ConvNeXt-dcls.
- **Depthwise implicit gemm:** this method can significantly increase throughput in the case of very large dilated kernel sizes. In our experiments, the largest dilated kernel size is 17, and therefore this method is not absolutely necessary. However, the DCLS user can choose to use it instead of the native method, which improves the throughput.

4 RESULTS AND DISCUSSION

4.1 SETTINGS

We started with an exploratory study on ResNet-50, where we drop-in replaced all the 3×3 convolutions of the model by 2D-DCLS ones. For that, we used a lightweight procedure named the

“A3 configuration”, described in Wightman et al. (2021). We then moved to the ConvNeXt models, where we limited our studies to its three first variants namely: the tiny, the small and the base models with input crops of size 224×224 (Liu et al., 2022b). Here, we drop-in replaced all the depthwise convolutions of the model by DCLS ones. We reconducted all the experiments, and evaluated the seed sensitivity for the ConvNeXt-dcls model by calculating the standard deviation of the top-1 accuracy on three different seeds, for the tiny variant. We found the standard deviation to be ± 0.04 , which is compatible with what was found in Liu et al. (2022b). Given this reasonably low variability, the remaining experiments were done on one seed only.

4.2 EMPIRICAL EVALUATIONS ON IMAGENET1K

In the following, we report the top-1 accuracies found on the ImageNet1k validation dataset (Deng et al., 2009), using ImageNet1k training dataset only.

Using ResNet-50. Table 1 presents the results obtained for the ResNet-50 experiment using the A3 configuration. The aim of this study is not to exceed the state-of-the-art for this particular configuration, but rather to give a first experimental evidence of the relevance of the DCLS method with non-separable convolutions and with one of the most popular CNN architectures in computer vision.

We can observe that when using the standard dilated convolution, the results only get worse as we increase the dilation rate. Moreover, increasing the kernel size ($3 \rightarrow 7$) in the case of standard convolution increases the accuracy but at the expense of not only the throughput which decreases, but also of the number of parameters which triples.

With fewer parameters, the ResNet-50-dcls model manages to surpass the baseline but at the expense of the throughput. This last disadvantage is due to the fact that ResNet-50 uses non-separable convolutions. We will see in Table 2 that for the ConvNeXt model, this extra cost in throughput is minimized thanks to the depthwise separable convolution.

model	kernel size / count	dil	# param.	FLOPs	throughput (image / s)	Top-1 acc. (crop 160)
ResNet-50	3/9	1	25.6M	4.1G	1021.9	75.8
ResNet-50	7/49	1	75.9M	12.3G	642.6	77.0
ResNet-50	3/9	2	25.6M	4.1G	931.8	71.7
ResNet-50	3/9	3	25.6M	4.1G	943.4	70.1
ResNet50-dcls ●	7/5	–	24.0M	12.3G	627.2	76.5
ResNet50-dcls ●	7/6	–	26.0M	12.3G	627.1	76.5

Table 1: **Classification accuracy on ImageNet-1K using ResNet-50.** The throughput was calculated at inference time, on image crops of size 224×224 using a single V100-32gb gpu. When the model contains DCLS convolutions we reported the kernel count and dilated kernel size. Otherwise, the kernel size is reported and thus the kernel count is in fact the square of that parameter.

Using ConvNeXt. We present numerically in Table 2 and graphically in Fig. 1, the results obtained for ConvNeXt using the settings for ImageNet1k training with input crops of size 224×224 , as described in Liu et al. (2022b): Table 5. We replaced ConvNeXt’s depthwise separable convolutions (of kernel size 7×7), by DCLS2d ones of dilated kernel size 17×17 and of kernel count equal to 34 for the tiny variant, and 40 for the small and base variants. We used all the techniques previously described in Section 3 during training. From Table 2, we highlight the fact that ConvNeXt with DCLS convolutions always surpasses the ConvNeXt baseline in accuracy (gains ranging from 0.3 to 0.6) with the same number of parameters and only a little cost on throughput. We think that this gain in accuracy is remarkable, given that we only replaced the depthwise convolutional layers, which represent just about 1% of the total number of parameters and 2% of the total number of FLOPs in ConvNeXt models. ConvNeXt model with a standard dilation of rate 2 performed poorly (see ConvNeXt-T-dil2). SLaK model performs about as well as DCLS but with a higher cost on throughput and parameters count.

DCLS can be seen as a kernel reparametrization technique that reduces the number of trainable parameters. For example, in the case of ConvNeXt-T-dcls, a 17×17 kernel (289 parameters) is parameterized by 34 triplets (x-position, y-position, weight), i.e. 102 parameters. The kernels that could be represented by the DCLS reparametrization constitute a subset of all possible dense kernels. In fact, by learning the suitable weights during training, a dense kernel could implement any DCLS one. It may therefore be counter-intuitive that DCLS leads to higher accuracy than a dense 17×17 convolution layer (see ConvNeXt-T-ker17). The problem with dense convolutional layers having large kernel sizes is that the number of trainable parameters is huge, which makes learning impractical.

Finally, we observe that after training, the DCLS position density is higher around the center of the RF (see Appendix D), suggesting that the central region is the most important one. Conversely, DC samples the whole RF uniformly, which is most likely sub-optimal, and that could explain its poor performance.

model	image size	# param.	FLOPs	throughput (image / s)	Top-1 acc.
Swin-T	224^2	28M	4.5G	757.9	81.3
ConvNeXt-T ●	224^2	29M	4.5G	774.7	82.1
ConvNeXt-T-dil2	224^2	29M	4.5G	773.6	80.8
ConvNeXt-T-ker17	224^2	30M	5G	560.0	82.0
SLaK-T ●●	224^2	30M ● / 38M ●	9.4G	583.5	82.5
ConvNeXt-T-dcls ●	224^2	29M	5.0G	725.3	82.5
Swin-S	224^2	50M	8.7G	436.7	83.0
ConvNeXt-S ●	224^2	50M	8.7G	447.1	83.1
SLaK-S ●●	224^2	55M ● / 75M ●	16.6G	367.9	83.8
ConvNeXt-S-dcls ●	224^2	50M	9.5G	433.4	83.7
Swin-B	224^2	88M	15.4G	286.6	83.5
ConvNeXt-B ●	224^2	89M	15.4G	292.1	83.8
RepLKNet-31B ●	224^2	79M	15.4G	295.5	83.5
SLaK-B ●●	224^2	95M ● / 122M ●	25.9G	245.4	84.0
ConvNeXt-B-dcls ●	224^2	89M	16.5G	285.4	84.1

Table 2: **Classification accuracy on ImageNet-1K.** The inference throughput was calculated using a single V100-32gb gpu and scaled to take into account all the optimizations used in Liu et al. (2022b). For the SLaK model, we report both the effective number of parameters returned by Pytorch ● and the one reported in Liu et al. (2022a) ●, that takes sparsity into account. The calculated FLOPs for this last model are different from the ones reported in Liu et al. (2022a), as we took the implicit gemm FLOPs into account.

4.3 EMPIRICAL EVALUATION ON DOWNSTREAM AND ROBUSTNESS TASKS

We now report the results found for semantic segmentation on the ADE20K dataset (Zhou et al., 2019) and for object detection on the COCO dataset (Lin et al., 2014) using ConvNeXt-dcls backbones. In addition, we present the results found for robustness tasks consisting on directly testing (without further tuning) the previously obtained ConvNeXt-dcls backbones on the following robustness benchmarks: ImageNet-C/ \bar{C} /A/R/Sketch (Hendrycks & Dietterich, 2019; Mintun et al., 2021; Hendrycks et al., 2021b;a; Wang et al., 2019).

Semantic segmentation on ADE20k. The results obtained in semantic segmentation show an improvement in performance by the ConvNeXt-dcls tiny and base backbones with equal number of parameters and FLOPs (Table 3). As in Liu et al. (2021) and Bao et al. (2021), we evaluated the mIoU with single scale testing and used the exact same configurations as in Liu et al. (2022b).

Object detection and segmentation on COCO. All ConvNeXt-dcls backbones have shown a noticeable improvement in average accuracy on both the object detection and segmentation tasks on the COCO dataset, again at iso-parameters and iso-FLOPS (Table 4). We only tested with Cascade

backbone	input crop.	mIoU (ss)	# param.	FLOPs
ConvNeXt-T ●	512 ²	46.0	60M	939G
SLaK-T ●	512 ²	47.1	65M	945G
ConvNeXt-T-dcls ●	512 ²	47.1	60M	950G
ConvNeXt-S ●	512 ²	48.7	82M	1027G
ConvNeXt-S-dcls ●	512 ²	48.4	82M	1045G
ConvNeXt-B ●	512 ²	49.1	122M	1170G
ConvNeXt-B-dcls ●	512 ²	49.3	122M	1193G

Table 3: **ADE20K validation results** using UperNet (Xiao et al., 2018). We report mIoU results with single scale testing. FLOPs are based on input sizes of (2048, 512).

Mask-RCNN Cai & Vasconcelos (2018) and used the exact same configurations as in Liu et al. (2022b).

backbone	FLOPs	AP ^{box}	AP ₅₀ ^{box}	AP ₇₅ ^{box}	AP ^{mask}	AP ₅₀ ^{mask}	AP ₇₅ ^{mask}
Cascade Mask-RCNN 3 × schedule							
ResNet-50	739G	46.3	64.3	50.5	40.1	61.7	43.4
X101-32	819G	48.1	66.5	52.4	41.6	63.9	45.2
X101-64	972G	48.3	66.4	52.3	41.7	64.0	45.1
Swin-T	745G	50.4	69.2	54.7	43.7	66.6	47.3
ConvNeXt-T ●	741G	50.4	69.1	54.8	43.7	66.5	47.3
ConvNeXt-dcls-T ●	751G	51.2	69.9	55.7	44.5	67.5	48.3
Swin-S	838G	51.9	70.7	56.3	45.0	68.2	48.8
ConvNeXt-S ●	827G	51.9	70.8	56.5	45.0	68.4	49.1
ConvNeXt-dcls-S ●	844G	52.8	71.6	57.6	45.6	69.0	49.3
Swin-B	982G	51.9	70.5	56.4	45.0	68.1	48.9
ConvNeXt-B ●	964G	52.7	71.3	57.2	45.6	68.9	49.5
ConvNeXt-dcls-B ●	987G	53.0	71.5	57.7	46.0	69.3	50.0

Table 4: **COCO object detection and segmentation results** using Cascade Mask-RCNN. Average Precision of the ResNet-50 and X101 models are from (Liu et al., 2021). FLOPs are calculated with image size (1280, 800).

Robustness Evaluation on ImageNet-C/ \bar{C} /A/R/Sketch. ConvNeXt-dcls backbones show very good performances when it comes to robustness. This is illustrated by the results obtained for the different benchmarks we have tried and for which we have reconducted the experiments. All of them show a gain in classification accuracy with DCLS, except SK with the S model (Table 5).

Model	FLOPs / Params	Clean	C(↓)	\bar{C} (↓)	A	R	SK
ResNet-50	4.1/25.6	76.1	76.7	57.7	0.0	36.1	24.1
ConvNeXt-T ●	4.5/28.6	82.1	41.6	41.2	23.5	47.6	33.8
ConvNeXt-dcls-T ●	5.0/28.6	82.5	41.5	39.7	23.9	47.8	34.7
ConvNeXt-S ●	8.7/50.2	83.1	38.9	37.8	30.1	50.1	37.1
ConvNeXt-dcls-S ●	9.5/50.2	83.7	37.8	35.2	33.7	50.4	36.7
ConvNeXt-B ●	15.4/88.6	83.8	37.0	35.7	35.5	51.7	38.2
ConvNeXt-dcls-B ●	16.5/88.6	84.1	36.3	34.3	36.8	52.6	38.4

Table 5: **Robustness evaluation of ConvNeXt-dcls.** We reconducted this study for ConvNeXt. For ImageNet-C and ImageNet-Cbar, the error is reported rather than the accuracy. It was calculated for both datasets by taking the average error over 5 levels of noise severity and over all the noise categories available in the the datasets.

5 RELATED WORK

One of the works that motivated the DCLS method is that of the *effective receptive field* (ERF) (Luo et al., 2016), which characterizes how much each input pixel in a receptive field can impact the output of a unit in the downstream convolutional layers of a neural network, leading to the notion of an effective receptive field. Among the findings of this work the most relevant ones for ours are that not all pixels in a receptive field contribute equally to an output response, the kernel center has much larger impact and that the effective receptive field size increases linearly with the square root of convolutional layers. Given these findings, introducing a new degree of freedom by learning the positions of non-zero weights in dilated kernels might increase the expressive power of convolutional neural networks. A visual comparison between DCLS and non DCLS ERFs is available in Appendix F.

Several approaches for learning arbitrary geometric changes within the convolutional kernel have emerged, such as Felzenszwalb et al. (2008), Dai et al. (2017), Jia et al. (2016) and Zhou et al. (2021). Other notable techniques such as Chen et al. (2020) aggregate multiple parallel convolution kernels dynamically, while Su et al. (2019) make use of a multiplicative Gaussian filter to make the convolution content-adaptive. Those techniques are different from DCLS as the learned kernel dynamically relies on the input while in DCLS the kernel positions and weights are input agnostic. They are often quite efficient since they do not require any intermediate pre-processing of images to encode invariant features (Mumuni & Mumuni, 2021), and are of particular interest in classification, but even more in downstream tasks such as instance segmentation (Wang et al., 2020).

6 CONCLUSION

In this work, we proposed DCLS, a new dilated convolution method where the positions of non-zero kernel elements are made learnable via backpropagation. The non-differentiability issue of learning discrete positions was circumvented by interpolation. We demonstrated that DCLS often outperforms the standard and the dilated convolution. We listed a number of techniques that improve the learning process of DCLS, in particular sharing the positions within stages was key. We provided evidence that searching for optimal positions of weights within a dilated kernel can improve not only the accuracy in image classification, but also in downstream and robustness tasks, using existing CNN architectures, without increasing their number of parameters. We reported a throughput overhead introduced by DCLS, but it remains marginal, provided that we use CNN architectures involving separable convolutions, which is the case for most modern CNNs, such as ConvNeXts.

Future work So far we have shown that DCLS can be used to drop-in replace standard convolution layers in existing architectures. We now would like to search for an architecture dedicated to DCLS, that would get the maximum benefit out of the method. Recent CNN-related works such as Re-pLKNet, make use of large kernels using a re-parameterizing trick, we might explore this direction to further enhance DCLS. Finally, we wish to show that the method is also of interest in 1D and 3D use cases.

ACKNOWLEDGMENTS

This work was performed using HPC resources from GENCI-IDRIS (Grant 2021-[AD011013219]) and from CALMIP (Grant 2021-[P21052]). Support from the ANR-3IA Artificial and Natural Intelligence Toulouse Institute is gratefully acknowledged. We would also like to thank the region of Toulouse Occitanie.

REFERENCES

- André Araujo, Wade Norris, and Jack Sim. Computing receptive fields of convolutional neural networks. *Distill*, 2019. doi: 10.23915/distill.00021. <https://distill.pub/2019/computing-receptive-fields>.
- Hangbo Bao, Li Dong, and Furu Wei. Beit: Bert pre-training of image transformers. *arXiv preprint arXiv:2106.08254*, 2021.

-
- Zhaowei Cai and Nuno Vasconcelos. Cascade r-cnn: Delving into high quality object detection. In *Proc. IEEE/CVF Conf. Comput. Vis. Pattern Recog. (CVPR)*, pp. 6154–6162, 2018.
- Liang-Chieh Chen, George Papandreou, Iasonas Kokkinos, Kevin Murphy, and Alan L Yuille. Deeplab: Semantic image segmentation with deep convolutional nets, atrous convolution, and fully connected CRFs. *IEEE Trans. Pattern Anal. Mach. Intell.*, 40(4):834–848, 2017.
- Liang-Chieh Chen, Yukun Zhu, George Papandreou, Florian Schroff, and Hartwig Adam. Encoder-decoder with atrous separable convolution for semantic image segmentation. In *Proc. Eur. Conf. Comput. Vis. (ECCV)*, pp. 801–818, 2018.
- Yinpeng Chen, Xiyang Dai, Mengchen Liu, Dongdong Chen, Lu Yuan, and Zicheng Liu. Dynamic convolution: Attention over convolution kernels. In *Proc. IEEE/CVF Conf. Comput. Vis. Pattern Recog. (CVPR)*, pp. 11030–11039, 2020.
- Jifeng Dai, Haozhi Qi, Yuwen Xiong, Yi Li, Guodong Zhang, Han Hu, and Yichen Wei. Deformable convolutional networks. In *Int. Conf. Comput. Vis.*, pp. 764–773, 2017.
- Jia Deng, Wei Dong, Richard Socher, Li-Jia Li, Kai Li, and Li Fei-Fei. Imagenet: A large-scale hierarchical image database. In *Proc. IEEE/CVF Conf. Comput. Vis. Pattern Recog. (CVPR)*, pp. 248–255. IEEE, 2009.
- Xiaohan Ding, Xiangyu Zhang, Jungong Han, and Guiguang Ding. Scaling up your kernels to 31x31: Revisiting large kernel design in CNNs. In *Proc. IEEE/CVF Conf. Comput. Vis. Pattern Recog. (CVPR)*, pp. 11963–11975, 2022.
- Alexey Dosovitskiy, Lucas Beyer, Alexander Kolesnikov, Dirk Weissenborn, Xiaohua Zhai, Thomas Unterthiner, Mostafa Dehghani, Matthias Minderer, Georg Heigold, Sylvain Gelly, et al. An image is worth 16x16 words: Transformers for image recognition at scale. *arXiv preprint arXiv:2010.11929*, 2020.
- Pedro Felzenszwalb, David McAllester, and Deva Ramanan. A discriminatively trained, multiscale, deformable part model. In *Proc. IEEE/CVF Conf. Comput. Vis. Pattern Recog. (CVPR)*, pp. 1–8. IEEE, 2008.
- Kaiming He, Xiangyu Zhang, Shaoqing Ren, and Jian Sun. Deep residual learning for image recognition. In *Proc. IEEE/CVF Conf. Comput. Vis. Pattern Recog. (CVPR)*, pp. 770–778, 2016.
- Dan Hendrycks and Thomas Dietterich. Benchmarking neural network robustness to common corruptions and perturbations. *arXiv preprint arXiv:1903.12261*, 2019.
- Dan Hendrycks, Steven Basart, Norman Mu, Saurav Kadavath, Frank Wang, Evan Dorundo, Rahul Desai, Tyler Zhu, Samyak Parajuli, Mike Guo, et al. The many faces of robustness: A critical analysis of out-of-distribution generalization. In *Int. Conf. Comput. Vis.*, pp. 8340–8349, 2021a.
- Dan Hendrycks, Kevin Zhao, Steven Basart, Jacob Steinhardt, and Dawn Song. Natural adversarial examples. In *Proc. IEEE/CVF Conf. Comput. Vis. Pattern Recog. (CVPR)*, pp. 15262–15271, 2021b.
- Matthias Holschneider, Richard Kronland-Martinet, Jean Morlet, and Ph Tchamitchian. A real-time algorithm for signal analysis with the help of the wavelet transform. In *Wavelets*, pp. 286–297. Springer, 1990.
- Xu Jia, Bert De Brabandere, Tinne Tuytelaars, and Luc V Gool. Dynamic filter networks. *Proc. Adv. Neural Inform. Process. Syst. (NIPS)*, 29, 2016.
- Tsung-Yi Lin, Michael Maire, Serge Belongie, James Hays, Pietro Perona, Deva Ramanan, Piotr Dollár, and C Lawrence Zitnick. Microsoft coco: Common objects in context. In *Proc. Eur. Conf. Comput. Vis. (ECCV)*, pp. 740–755. Springer, 2014.
- Shiwei Liu, Tianlong Chen, Xiaohan Chen, Xuxi Chen, Qiao Xiao, Boqian Wu, Mykola Pechenizkiy, Decebal Mocanu, and Zhangyang Wang. More ConvNets in the 2020s: Scaling up Kernels Beyond 51x51 using Sparsity. *arXiv preprint arXiv:2207.03620*, 2022a.

-
- Ze Liu, Yutong Lin, Yue Cao, Han Hu, Yixuan Wei, Zheng Zhang, Stephen Lin, and Baining Guo. Swin transformer: Hierarchical vision transformer using shifted windows. In *Int. Conf. Comput. Vis.*, pp. 10012–10022, 2021.
- Zhuang Liu, Hanzi Mao, Chao-Yuan Wu, Christoph Feichtenhofer, Trevor Darrell, and Saining Xie. A convnet for the 2020s. In *Proc. IEEE/CVF Conf. Comput. Vis. Pattern Recog. (CVPR)*, pp. 11976–11986, 2022b.
- Xin Lu, Buyu Li, Yuxin Yue, Quanquan Li, and Junjie Yan. Grid R-CNN. In *Proc. IEEE/CVF Conf. Comput. Vis. Pattern Recog. (CVPR)*, pp. 7363–7372, 2019.
- Wenjie Luo, Yujia Li, Raquel Urtasun, and Richard Zemel. Understanding the effective receptive field in deep convolutional neural networks. In *Proc. Adv. Neural Inform. Process. Syst. (NIPS)*, pp. 4905–4913, 2016.
- Eric Mintun, Alexander Kirillov, and Saining Xie. On interaction between augmentations and corruptions in natural corruption robustness. *Proc. Adv. Neural Inform. Process. Syst. (NIPS)*, 34: 3571–3583, 2021.
- Alhassan Mumuni and Fuseini Mumuni. Cnn architectures for geometric transformation-invariant feature representation in computer vision: A review. *SN Computer Science*, 2(5):1–23, 2021.
- Mark Sandler, Andrew Howard, Menglong Zhu, Andrey Zhmoginov, and Liang-Chieh Chen. Mobilenetv2: Inverted residuals and linear bottlenecks. In *Proc. IEEE/CVF Conf. Comput. Vis. Pattern Recog. (CVPR)*, pp. 4510–4520, 2018.
- Mark J Shensa. The discrete wavelet transform: wedding the a trous and mallat algorithms. *IEEE Trans. Signal Process.*, 40(10):2464–2482, 1992.
- Hang Su, Varun Jampani, Deqing Sun, Orazio Gallo, Erik Learned-Miller, and Jan Kautz. Pixel-adaptive convolutional neural networks. In *Proc. IEEE/CVF Conf. Comput. Vis. Pattern Recog. (CVPR)*, pp. 11166–11175, 2019.
- Hugues Thomas, Charles R. Qi, Jean-Emmanuel Deschaud, Beatriz Marcotegui, François Goulette, and Leonidas J. Guibas. Kpconv: Flexible and deformable convolution for point clouds. *Int. Conf. Comput. Vis.*, 2019.
- Asher Trockman and J Zico Kolter. Patches are all you need? *arXiv preprint arXiv:2201.09792*, 2022.
- Haohan Wang, Songwei Ge, Zachary Lipton, and Eric P Xing. Learning robust global representations by penalizing local predictive power. *Proc. Adv. Neural Inform. Process. Syst. (NIPS)*, 32, 2019.
- Xinlong Wang, Rufeng Zhang, Tao Kong, Lei Li, and Chunhua Shen. Solov2: Dynamic and fast instance segmentation. *Proc. Adv. Neural Inform. Process. Syst. (NIPS)*, 33:17721–17732, 2020.
- Zhengyang Wang and Shuiwang Ji. Smoothed dilated convolutions for improved dense prediction. In *Proceedings of the 24th ACM SIGKDD International Conference on Knowledge Discovery & Data Mining*, pp. 2486–2495, 2018.
- Ross Wightman, Hugo Touvron, and Hervé Jégou. Resnet strikes back: An improved training procedure in timm. *arXiv preprint arXiv:2110.00476*, 2021.
- Tete Xiao, Yingcheng Liu, Bolei Zhou, Yuning Jiang, and Jian Sun. Unified perceptual parsing for scene understanding. In *Proc. Eur. Conf. Comput. Vis. (ECCV)*, pp. 418–434, 2018.
- Fisher Yu and Vladlen Koltun. Multi-scale context aggregation by dilated convolutions. *arXiv preprint arXiv:1511.07122*, 2015.
- Fisher Yu, Vladlen Koltun, and Thomas Funkhouser. Dilated residual networks. In *Proc. IEEE/CVF Conf. Comput. Vis. Pattern Recog. (CVPR)*, pp. 472–480, 2017.

Bolei Zhou, Hang Zhao, Xavier Puig, Tete Xiao, Sanja Fidler, Adela Barriuso, and Antonio Torralba. Semantic understanding of scenes through the ade20k dataset. *Int. J. Comput. Vis.*, 127(3):302–321, 2019.

Jingkai Zhou, Varun Jampani, Zhixiong Pi, Qiong Liu, and Ming-Hsuan Yang. Decoupled dynamic filter networks. In *Proc. IEEE/CVF Conf. Comput. Vis. Pattern Recog. (CVPR)*, pp. 6647–6656, 2021.

A APPENDIX: PROOFS AND DERIVATION FOR THE SCALAR WEIGHT CASE

This is a detailed proof for the result of section 2.2.

Let us consider two column vectors $\mathbf{x} = [x_1 \ x_2 \ \dots \ x_{s_1}]^T$ of \mathbb{R}^{s_1} and $\mathbf{y} = [y_1 \ y_2 \ \dots \ y_{s_2}]^T$ of \mathbb{R}^{s_2} . We have:

$$\mathbf{x}^T f(w, p^1, p^2) \mathbf{y} = \sum_{i=1}^{s_1} \sum_{j=1}^{s_2} \mathbf{K}_{ij} x_i y_j \quad (20)$$

Since \mathbf{K} is zero except for the 4 aforementioned positions, we have

$$\begin{aligned} \mathbf{x}^T f(w, p^1, p^2) \mathbf{y} &= \mathbf{K}_{\lfloor p^1 \rfloor \lfloor p^2 \rfloor} x_{\lfloor p^1 \rfloor} y_{\lfloor p^2 \rfloor} \\ &\quad + \mathbf{K}_{\lfloor p^1 \rfloor + 1 \lfloor p^2 \rfloor} x_{\lfloor p^1 \rfloor + 1} y_{\lfloor p^2 \rfloor} \\ &\quad + \mathbf{K}_{\lfloor p^1 \rfloor \lfloor p^2 \rfloor + 1} x_{\lfloor p^1 \rfloor} y_{\lfloor p^2 \rfloor + 1} \\ &\quad + \mathbf{K}_{\lfloor p^1 \rfloor + 1 \lfloor p^2 \rfloor + 1} x_{\lfloor p^1 \rfloor + 1} y_{\lfloor p^2 \rfloor + 1} \end{aligned} \quad (21)$$

By deriving this expression with respect to w , p^1 and p^2 we obtain

$$\begin{aligned} \frac{\partial(\mathbf{x}^T f(w, p^1, p^2) \mathbf{y})}{\partial w} &= (1 - r^1) (1 - r^2) x_{\lfloor p^1 \rfloor} y_{\lfloor p^2 \rfloor} \\ &\quad + r^1 (1 - r^2) x_{\lfloor p^1 \rfloor + 1} y_{\lfloor p^2 \rfloor} \\ &\quad + (1 - r^1) r^2 x_{\lfloor p^1 \rfloor} y_{\lfloor p^2 \rfloor + 1} \\ &\quad + r^1 r^2 x_{\lfloor p^1 \rfloor + 1} y_{\lfloor p^2 \rfloor + 1} \end{aligned} \quad (22)$$

$$\begin{aligned} \frac{\partial(\mathbf{x}^T f(w, p^1, p^2) \mathbf{y})}{\partial p^1} &= w [- (1 - r^2) x_{\lfloor p^1 \rfloor} y_{\lfloor p^2 \rfloor} \\ &\quad + (1 - r^2) x_{\lfloor p^1 \rfloor + 1} y_{\lfloor p^2 \rfloor} \\ &\quad - r^2 x_{\lfloor p^1 \rfloor} y_{\lfloor p^2 \rfloor + 1} \\ &\quad + r^2 x_{\lfloor p^1 \rfloor + 1} y_{\lfloor p^2 \rfloor + 1}] \end{aligned} \quad (23)$$

$$\begin{aligned} \frac{\partial(\mathbf{x}^T f(w, p^1, p^2) \mathbf{y})}{\partial p^2} &= w [- (1 - r^1) x_{\lfloor p^1 \rfloor} y_{\lfloor p^2 \rfloor} \\ &\quad - r^1 x_{\lfloor p^1 \rfloor + 1} y_{\lfloor p^2 \rfloor} \\ &\quad + (1 - r^1) x_{\lfloor p^1 \rfloor} y_{\lfloor p^2 \rfloor + 1} \\ &\quad + r^1 x_{\lfloor p^1 \rfloor + 1} y_{\lfloor p^2 \rfloor + 1}] \end{aligned} \quad (24)$$

Because of the linearity of the differentiation in the three previous equations, we could write:

$$\frac{\partial(\mathbf{x}^T f(w, p^1, p^2) \mathbf{y})}{\partial w} = \mathbf{x}^T \frac{\partial f(w, p^1, p^2)}{\partial w} \mathbf{y} = \mathbf{x}^T \mathbf{G}_w \mathbf{y} \quad (25)$$

$$\frac{\partial(\mathbf{x}^T f(w, p^1, p^2) \mathbf{y})}{\partial p^1} = \mathbf{x}^T \frac{\partial f(w, p^1, p^2)}{\partial p^1} \mathbf{y} = \mathbf{x}^T \mathbf{G}_{p^1} \mathbf{y} \quad (26)$$

$$\frac{\partial(\mathbf{x}^T f(w, p^1, p^2) \mathbf{y})}{\partial p^2} = \mathbf{x}^T \frac{\partial f(w, p^1, p^2)}{\partial p^2} \mathbf{y} = \mathbf{x}^T \mathbf{G}_{p^2} \mathbf{y} \quad (27)$$

where \mathbf{G}_w , \mathbf{G}_{p^1} , \mathbf{G}_{p^2} , respectively stand for the s_1 by s_2 matrices described below and which have zeros everywhere except at the four positions of interpolation.

$$\mathbf{G}_w =$$

$$\begin{pmatrix} 0 & \cdots & \lfloor p^2 \rfloor & \lfloor p^2 \rfloor + 1 & \cdots & 0 \\ \vdots & \ddots & 0 & 0 & \ddots & \vdots \\ 0 & 0 & (1-r^1)(1-r^2) & r^2(1-r^1) & 0 & 0 \\ 0 & 0 & r^1(1-r^2) & r^1 r^2 & 0 & 0 \\ \vdots & \ddots & 0 & 0 & \ddots & \vdots \\ 0 & \cdots & 0 & 0 & \cdots & 0 \end{pmatrix} \begin{matrix} \lfloor p^1 \rfloor \\ \lfloor p^1 \rfloor + 1 \end{matrix} \quad (28)$$

$$\mathbf{G}_{p^1} =$$

$$\begin{pmatrix} 0 & \cdots & \lfloor p^2 \rfloor & \lfloor p^2 \rfloor + 1 & \cdots & 0 \\ \vdots & \ddots & 0 & 0 & \ddots & \vdots \\ 0 & 0 & -w(1-r^2) & -wr^2 & 0 & 0 \\ 0 & 0 & w(1-r^2) & wr^2 & 0 & 0 \\ \vdots & \ddots & 0 & 0 & \ddots & \vdots \\ 0 & \cdots & 0 & 0 & \cdots & 0 \end{pmatrix} \begin{matrix} \lfloor p^1 \rfloor \\ \lfloor p^1 \rfloor + 1 \end{matrix} \quad (29)$$

$$\mathbf{G}_{p^2} =$$

$$\begin{pmatrix} 0 & \cdots & \lfloor p^2 \rfloor & \lfloor p^2 \rfloor + 1 & \cdots & 0 \\ \vdots & \ddots & 0 & 0 & \ddots & \vdots \\ 0 & 0 & -w(1-r^1) & w(1-r^1) & 0 & 0 \\ 0 & 0 & -wr^1 & wr^1 & 0 & 0 \\ \vdots & \ddots & 0 & 0 & \ddots & \vdots \\ 0 & \cdots & 0 & 0 & \cdots & 0 \end{pmatrix} \begin{matrix} \lfloor p^1 \rfloor \\ \lfloor p^1 \rfloor + 1 \end{matrix} \quad (30)$$

From the three equations (25), (26) and (27), we can identify

$$\frac{\partial f(w, p^1, p^2)}{\partial w} = \mathbf{G}_w \quad (31)$$

$$\frac{\partial f(w, p^1, p^2)}{\partial p^1} = \mathbf{G}_{p^1} \quad (32)$$

$$\frac{\partial f(w, p^1, p^2)}{\partial p^2} = \mathbf{G}_{p^2} \quad (33)$$

Finally, we have

$$\begin{aligned} \frac{\partial loss}{\partial w} &= \mathbf{G} \times_{\mathbf{F}} \mathbf{G}_w = (1 - r^1) (1 - r^2) g_{\lfloor p^1 \rfloor \lfloor p^2 \rfloor} \\ &\quad + r^1 (1 - r^2) g_{\lfloor p^1 \rfloor + 1 \lfloor p^2 \rfloor} \\ &\quad + (1 - r^1) r^2 g_{\lfloor p^1 \rfloor \lfloor p^2 \rfloor + 1} \\ &\quad + r^1 r^2 g_{\lfloor p^1 \rfloor + 1 \lfloor p^2 \rfloor + 1} \end{aligned} \quad (34)$$

$$\begin{aligned} \frac{\partial loss}{\partial p^1} &= \mathbf{G} \times_{\mathbf{F}} \mathbf{G}_{p^1} = w [- (1 - r^2) g_{\lfloor p^1 \rfloor \lfloor p^2 \rfloor} \\ &\quad + (1 - r^2) g_{\lfloor p^1 \rfloor + 1 \lfloor p^2 \rfloor} \\ &\quad - r^2 g_{\lfloor p^1 \rfloor \lfloor p^2 \rfloor + 1} \\ &\quad + r^2 g_{\lfloor p^1 \rfloor + 1 \lfloor p^2 \rfloor + 1}] \end{aligned} \quad (35)$$

$$\begin{aligned} \frac{\partial loss}{\partial p^2} &= \mathbf{G} \times_{\mathbf{F}} \mathbf{G}_{p^2} = w [- (1 - r^1) g_{\lfloor p^1 \rfloor \lfloor p^2 \rfloor} \\ &\quad - r^1 g_{\lfloor p^1 \rfloor + 1 \lfloor p^2 \rfloor} \\ &\quad + (1 - r^1) g_{\lfloor p^1 \rfloor \lfloor p^2 \rfloor + 1} \\ &\quad + r^1 g_{\lfloor p^1 \rfloor + 1 \lfloor p^2 \rfloor + 1}] \end{aligned} \quad (36)$$

B APPENDIX: PROOFS AND DERIVATION FOR THE GENERAL 2D CASE

This is a detailed proof for the result of section 2.3.

By applying the chain rule we obtain

$\forall i \in \llbracket 1 .. m \rrbracket$:

$$\frac{\partial loss}{\partial w_i} = g'(F(\mathbf{w}, \mathbf{p}^1, \mathbf{p}^2)) \times_{\mathbf{F}} \frac{\partial F(\mathbf{w}, \mathbf{p}^1, \mathbf{p}^2)}{\partial w_i} \quad (37)$$

$$\frac{\partial loss}{\partial p_i^1} = g'(F(\mathbf{w}, \mathbf{p}^1, \mathbf{p}^2)) \times_{\mathbf{F}} \frac{\partial F(\mathbf{w}, \mathbf{p}^1, \mathbf{p}^2)}{\partial p_i^1} \quad (38)$$

$$\frac{\partial loss}{\partial p_i^2} = g'(F(\mathbf{w}, \mathbf{p}^1, \mathbf{p}^2)) \times_{\mathbf{F}} \frac{\partial F(\mathbf{w}, \mathbf{p}^1, \mathbf{p}^2)}{\partial p_i^2} \quad (39)$$

with

$$\begin{aligned} g'(F(\mathbf{w}, \mathbf{p}^1, \mathbf{p}^2)) &= \frac{\partial loss}{\partial \mathbf{K}} \\ &= \frac{\partial loss}{\partial F(\mathbf{w}, \mathbf{p}^1, \mathbf{p}^2)} \end{aligned} \quad (40)$$

Let us put

$$g'(F(\mathbf{w}, \mathbf{p}^1, \mathbf{p}^2)) = \mathbf{G} = \begin{bmatrix} g_{11} & g_{12} & \cdots & g_{1s_2} \\ g_{21} & \ddots & & g_{1s_2} \\ \vdots & & \ddots & \vdots \\ g_{s_1 1} & g_{12} & \cdots & g_{s_1 s_2} \end{bmatrix} \quad (41)$$

Hence,

$$\frac{\partial loss}{\partial w_i} = \mathbf{G} \times_{\mathbf{F}} \frac{\partial \sum_{i=1}^m f(w_i, p_i^1, p_i^2)}{\partial w_i} \quad (42)$$

$$\frac{\partial loss}{\partial p_i^1} = \mathbf{G} \times_{\mathbf{F}} \frac{\partial \sum_{i=1}^m f(w_i, p_i^1, p_i^2)}{\partial p_i^1} \quad (43)$$

$$\frac{\partial loss}{\partial p_i^2} = \mathbf{G} \times_{\mathbf{F}} \frac{\partial \sum_{i=1}^m f(w_i, p_i^1, p_i^2)}{\partial p_i^2} \quad (44)$$

And we know that

$\forall (i, j) \in \llbracket 1 \dots m \rrbracket^2$:

$$i \neq j \implies \frac{\partial f(w_j, p_j^1, p_j^2)}{\partial w_i} = \frac{\partial f(w_j, p_j^1, p_j^2)}{\partial p_i^1} = \frac{\partial f(w_j, p_j^1, p_j^2)}{\partial p_i^2} = 0$$

we can then deduce from (34), (35) and (36) the gradients of the loss function with respect to weights and positions in the general case:

$\forall i \in \llbracket 1 \dots m \rrbracket$:

$$\begin{aligned} \left(\frac{\partial loss}{\partial \mathbf{w}} \right)_i &= (1 - r_i^1) (1 - r_i^2) g_{\lfloor p_i^1 \rfloor \lfloor p_i^2 \rfloor} \\ &\quad + r_i^1 (1 - r_i^2) g_{\lfloor p_i^1 \rfloor + 1 \lfloor p_i^2 \rfloor} \\ &\quad + (1 - r_i^1) r_i^2 g_{\lfloor p_i^1 \rfloor \lfloor p_i^2 \rfloor + 1} \\ &\quad + r_i^1 r_i^2 g_{\lfloor p_i^1 \rfloor + 1 \lfloor p_i^2 \rfloor + 1} \end{aligned} \quad (45)$$

$$\begin{aligned} \left(\frac{\partial loss}{\partial \mathbf{p}^1} \right)_i &= w_i [- (1 - r_i^2) g_{\lfloor p_i^1 \rfloor \lfloor p_i^2 \rfloor} \\ &\quad + (1 - r_i^2) g_{\lfloor p_i^1 \rfloor + 1 \lfloor p_i^2 \rfloor} \\ &\quad - r_i^2 g_{\lfloor p_i^1 \rfloor \lfloor p_i^2 \rfloor + 1} \\ &\quad + r_i^2 g_{\lfloor p_i^1 \rfloor + 1 \lfloor p_i^2 \rfloor + 1}] \end{aligned} \quad (46)$$

$$\begin{aligned} \left(\frac{\partial loss}{\partial \mathbf{p}^2} \right)_i &= w_i [- (1 - r_i^1) g_{\lfloor p_i^1 \rfloor \lfloor p_i^2 \rfloor} \\ &\quad - r_i^1 g_{\lfloor p_i^1 \rfloor + 1 \lfloor p_i^2 \rfloor} \\ &\quad + (1 - r_i^1) g_{\lfloor p_i^1 \rfloor \lfloor p_i^2 \rfloor + 1} \\ &\quad + r_i^1 g_{\lfloor p_i^1 \rfloor + 1 \lfloor p_i^2 \rfloor + 1}] \end{aligned} \quad (47)$$

C APPENDIX: 1D-DCLS, 3D-DCLS

We denote respectively by $s_1, s_2, s_3 \in \mathbb{N}^* \times \mathbb{N}^* \times \mathbb{N}^*$, the sizes of the constructed kernel along the x-axis, y-axis and the z-axis. Moreover, the $n \times p \times q$ tensor space of third dimension is denoted $\mathbb{R}^{n \times p \times q}$.

The function f defined in (2) could be adapted in order to construct a suitable kernel for the 1D convolution in the scalar weight case as follows:

$$\begin{aligned} f_{1D} : \mathbb{R} \times \mathbb{R} &\rightarrow \mathbb{R}^s \\ w, p &\mapsto \mathbf{k} \end{aligned} \quad (48)$$

where $\forall i \in \llbracket 1 \dots s \rrbracket$:

$$\mathbf{k}_i = \begin{cases} w (1 - r) & \text{if } i = \lfloor p^1 \rfloor \\ w r & \text{if } i = \lfloor p^1 \rfloor + 1 \\ 0 & \text{else} \end{cases} \quad (49)$$

and where the fractional part is:

$$r = \{p\} = p - \lfloor p \rfloor \quad (50)$$

Following the same construction in section 2.3 we can show that the gradients of the loss function with respect to weights and positions in the general 1D case are:

$\forall i \in \llbracket 1 \dots m \rrbracket$:

$$\left(\frac{\partial \text{loss}}{\partial \mathbf{w}} \right)_i = (1 - r_i) g_{\lfloor p_i \rfloor} + r_i g_{\lfloor p_i \rfloor + 1} \quad (51)$$

$$\left(\frac{\partial \text{loss}}{\partial \mathbf{p}} \right)_i = w_i (g_{\lfloor p_i \rfloor + 1} - g_{\lfloor p_i \rfloor}) \quad (52)$$

Furthermore, we define the function f_{3D} , the suitable kernel construction function in the 3D convolution case, as such:

$$f: \mathbb{R} \times \mathbb{R} \times \mathbb{R} \times \mathbb{R} \rightarrow \mathbb{R}^{s_1 \times s_2 \times s_3} \quad (53)$$

$$w, p^1, p^2, p^3 \mapsto \mathbf{K}$$

where $\forall i \in \llbracket 1 \dots s_1 \rrbracket, \forall j \in \llbracket 1 \dots s_2 \rrbracket, \forall l \in \llbracket 1 \dots s_3 \rrbracket$:

$$\mathbf{K}_{ijl} = \begin{cases} w (1 - r^1) (1 - r^2) (1 - r^3) & \text{if } i = \lfloor p^1 \rfloor, j = \lfloor p^2 \rfloor, l = \lfloor p^3 \rfloor \\ w r^1 (1 - r^2) (1 - r^3) & \text{if } i = \lfloor p^1 \rfloor + 1, j = \lfloor p^2 \rfloor, l = \lfloor p^3 \rfloor \\ w (1 - r^1) r^2 (1 - r^3) & \text{if } i = \lfloor p^1 \rfloor, j = \lfloor p^2 \rfloor + 1, l = \lfloor p^3 \rfloor \\ w r^1 r^2 (1 - r^3) & \text{if } i = \lfloor p^1 \rfloor + 1, j = \lfloor p^2 \rfloor + 1, l = \lfloor p^3 \rfloor \\ w (1 - r^1) (1 - r^2) r^3 & \text{if } i = \lfloor p^1 \rfloor, j = \lfloor p^2 \rfloor, l = \lfloor p^3 \rfloor + 1 \\ w r^1 (1 - r^2) r^3 & \text{if } i = \lfloor p^1 \rfloor + 1, j = \lfloor p^2 \rfloor, l = \lfloor p^3 \rfloor + 1 \\ w (1 - r^1) r^2 r^3 & \text{if } i = \lfloor p^1 \rfloor, j = \lfloor p^2 \rfloor + 1, l = \lfloor p^3 \rfloor + 1 \\ w r^1 r^2 r^3 & \text{if } i = \lfloor p^1 \rfloor + 1, j = \lfloor p^2 \rfloor + 1, l = \lfloor p^3 \rfloor + 1 \\ 0 & \text{else} \end{cases} \quad (54)$$

and where the fractional parts are:

$$\begin{aligned} r^1 &= \{p^1\} = p^1 - \lfloor p^1 \rfloor \\ r^2 &= \{p^2\} = p^2 - \lfloor p^2 \rfloor \\ r^3 &= \{p^3\} = p^3 - \lfloor p^3 \rfloor \end{aligned} \quad (55)$$

We can show that the gradients of the loss function with respect to weights and positions in the general 3D case are:

$\forall i \in \llbracket 1 .. m \rrbracket$:

$$\begin{aligned}
\left(\frac{\partial loss}{\partial \mathbf{w}}\right)_i &= (1 - r_i^1) (1 - r_i^2) (1 - r_i^3) g_{\lfloor p_i^1 \rfloor \lfloor p_i^2 \rfloor \lfloor p_i^3 \rfloor} \\
&\quad + r_i^1 (1 - r_i^2) (1 - r_i^3) g_{\lfloor p_i^1 \rfloor + 1 \lfloor p_i^2 \rfloor \lfloor p_i^3 \rfloor} \\
&\quad + (1 - r_i^1) r_i^2 (1 - r_i^3) g_{\lfloor p_i^1 \rfloor \lfloor p_i^2 \rfloor + 1 \lfloor p_i^3 \rfloor} \\
&\quad + r_i^1 r_i^2 (1 - r_i^3) g_{\lfloor p_i^1 \rfloor + 1 \lfloor p_i^2 \rfloor + 1 \lfloor p_i^3 \rfloor} \\
&\quad + (1 - r_i^1) (1 - r_i^2) r_i^3 g_{\lfloor p_i^1 \rfloor \lfloor p_i^2 \rfloor \lfloor p_i^3 \rfloor + 1} \\
&\quad + r_i^1 (1 - r_i^2) r_i^3 g_{\lfloor p_i^1 \rfloor + 1 \lfloor p_i^2 \rfloor \lfloor p_i^3 \rfloor + 1} \\
&\quad + (1 - r_i^1) r_i^2 r_i^3 g_{\lfloor p_i^1 \rfloor \lfloor p_i^2 \rfloor + 1 \lfloor p_i^3 \rfloor + 1} \\
&\quad + r_i^1 r_i^2 r_i^3 g_{\lfloor p_i^1 \rfloor + 1 \lfloor p_i^2 \rfloor + 1 \lfloor p_i^3 \rfloor + 1}
\end{aligned} \tag{56}$$

$$\begin{aligned}
\left(\frac{\partial loss}{\partial p^1}\right)_i &= w_i [- (1 - r_i^2) (1 - r_i^3) g_{\lfloor p_i^1 \rfloor \lfloor p_i^2 \rfloor \lfloor p_i^3 \rfloor} \\
&\quad + (1 - r_i^2) (1 - r_i^3) g_{\lfloor p_i^1 \rfloor + 1 \lfloor p_i^2 \rfloor \lfloor p_i^3 \rfloor} \\
&\quad - r_i^2 (1 - r_i^3) g_{\lfloor p_i^1 \rfloor \lfloor p_i^2 \rfloor + 1 \lfloor p_i^3 \rfloor} \\
&\quad + r_i^2 (1 - r_i^3) g_{\lfloor p_i^1 \rfloor + 1 \lfloor p_i^2 \rfloor + 1 \lfloor p_i^3 \rfloor} \\
&\quad - (1 - r_i^2) r_i^3 g_{\lfloor p_i^1 \rfloor \lfloor p_i^2 \rfloor \lfloor p_i^3 \rfloor + 1} \\
&\quad + (1 - r_i^2) r_i^3 g_{\lfloor p_i^1 \rfloor + 1 \lfloor p_i^2 \rfloor \lfloor p_i^3 \rfloor + 1} \\
&\quad - r_i^2 r_i^3 g_{\lfloor p_i^1 \rfloor \lfloor p_i^2 \rfloor + 1 \lfloor p_i^3 \rfloor + 1} \\
&\quad + r_i^2 r_i^3 g_{\lfloor p_i^1 \rfloor + 1 \lfloor p_i^2 \rfloor + 1 \lfloor p_i^3 \rfloor + 1}]
\end{aligned} \tag{57}$$

$$\begin{aligned}
\left(\frac{\partial loss}{\partial p^2}\right)_i &= w_i [- (1 - r_i^1) (1 - r_i^3) g_{\lfloor p_i^1 \rfloor \lfloor p_i^2 \rfloor \lfloor p_i^3 \rfloor} \\
&\quad - r_i^1 (1 - r_i^3) g_{\lfloor p_i^1 \rfloor + 1 \lfloor p_i^2 \rfloor \lfloor p_i^3 \rfloor} \\
&\quad + (1 - r_i^1) (1 - r_i^3) g_{\lfloor p_i^1 \rfloor \lfloor p_i^2 \rfloor + 1 \lfloor p_i^3 \rfloor} \\
&\quad + r_i^1 (1 - r_i^3) g_{\lfloor p_i^1 \rfloor + 1 \lfloor p_i^2 \rfloor + 1 \lfloor p_i^3 \rfloor} \\
&\quad - (1 - r_i^1) r_i^3 g_{\lfloor p_i^1 \rfloor \lfloor p_i^2 \rfloor \lfloor p_i^3 \rfloor + 1} \\
&\quad - r_i^1 r_i^3 g_{\lfloor p_i^1 \rfloor + 1 \lfloor p_i^2 \rfloor \lfloor p_i^3 \rfloor + 1} \\
&\quad + (1 - r_i^1) r_i^3 g_{\lfloor p_i^1 \rfloor \lfloor p_i^2 \rfloor + 1 \lfloor p_i^3 \rfloor + 1} \\
&\quad + r_i^1 r_i^3 g_{\lfloor p_i^1 \rfloor + 1 \lfloor p_i^2 \rfloor + 1 \lfloor p_i^3 \rfloor + 1}]
\end{aligned} \tag{58}$$

$$\begin{aligned}
\left(\frac{\partial loss}{\partial p^3}\right)_i &= w_i [- (1 - r_i^1) (1 - r_i^2) g_{\lfloor p_i^1 \rfloor \lfloor p_i^2 \rfloor \lfloor p_i^3 \rfloor} \\
&\quad - r_i^1 (1 - r_i^2) g_{\lfloor p_i^1 \rfloor + 1 \lfloor p_i^2 \rfloor \lfloor p_i^3 \rfloor} \\
&\quad - (1 - r_i^1) r_i^2 g_{\lfloor p_i^1 \rfloor \lfloor p_i^2 \rfloor + 1 \lfloor p_i^3 \rfloor} \\
&\quad - r_i^1 r_i^2 g_{\lfloor p_i^1 \rfloor + 1 \lfloor p_i^2 \rfloor + 1 \lfloor p_i^3 \rfloor} \\
&\quad + (1 - r_i^1) (1 - r_i^2) g_{\lfloor p_i^1 \rfloor \lfloor p_i^2 \rfloor \lfloor p_i^3 \rfloor + 1} \\
&\quad + r_i^1 (1 - r_i^2) g_{\lfloor p_i^1 \rfloor + 1 \lfloor p_i^2 \rfloor \lfloor p_i^3 \rfloor + 1} \\
&\quad + (1 - r_i^1) r_i^2 g_{\lfloor p_i^1 \rfloor \lfloor p_i^2 \rfloor + 1 \lfloor p_i^3 \rfloor + 1} \\
&\quad + r_i^1 r_i^2 g_{\lfloor p_i^1 \rfloor + 1 \lfloor p_i^2 \rfloor + 1 \lfloor p_i^3 \rfloor + 1}]
\end{aligned} \tag{59}$$

D APPENDIX: HISTOGRAMS OF POSITIONS

In the following, we show as histograms over training epochs, the distribution of the four kernel positions for the 2D-DCLS convolutions of the ConvNeXt-T-dcls model. Note that there is no agglutination or edge effect around the kernel limits, and that the distributions are relatively stable, with a higher concentration around the center of the kernel. Individual positions, however, are constantly moving; see animation at:

<https://wandb.ai/dcls/convnext/reports/Dcls-4--VmlldzoyMTQzMzAy?accessToken=pmg5nj0ywue9pwvzn4d7900mcq1129s0yfo5sjtocejhvnrkyszoyttlbyhgoqiy0>.

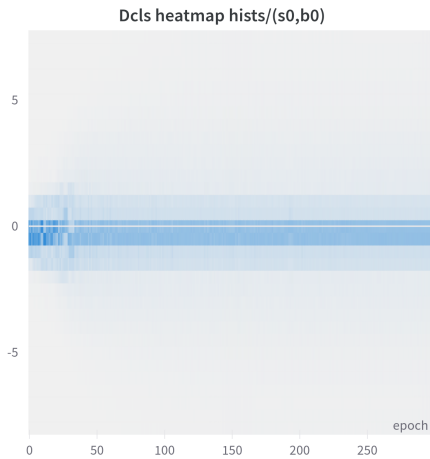


Figure 3: The distribution over epochs of kernel positions for the stage 0 of the ConvNeXt-T-dcls model.

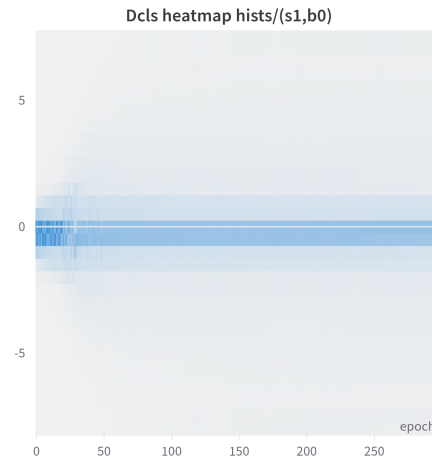


Figure 4: Idem for stage 1.

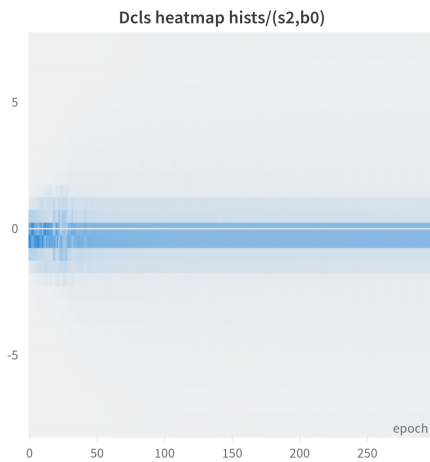


Figure 5: Idem for stage 2.

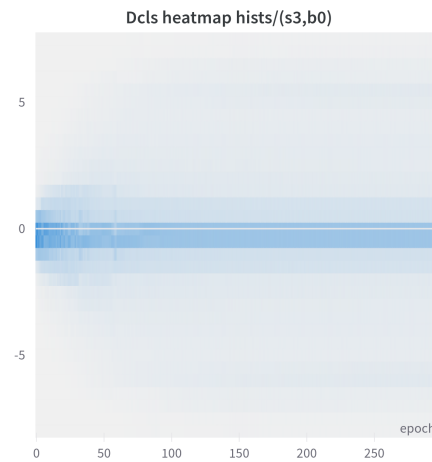


Figure 6: Idem for stage 3.

E APPENDIX: SPEED CURVES AND LEARNING RATE SCHEDULE

Here, we plot the average speed curves of the four position tensors for the 2D-DCLS convolutions $V_{\mathbf{p}}$ of the ConvNeXt-T-dcls model as functions of the training epochs. The general formula for the average speed of a DCLS position tensor of size $(cout, cin, m) \in \mathbb{N}^3$, at epoch t , is as follows:

$$\forall t \in \llbracket 1 .. t_{max} \rrbracket: \quad V_{\mathbf{p}}(t) = \frac{1}{cout \cdot cin \cdot m} \sum_{k=1}^{cout} \sum_{j=1}^{cin} \sum_{i=1}^m |P_{ijk}^t - P_{ijk}^{t-1}|$$

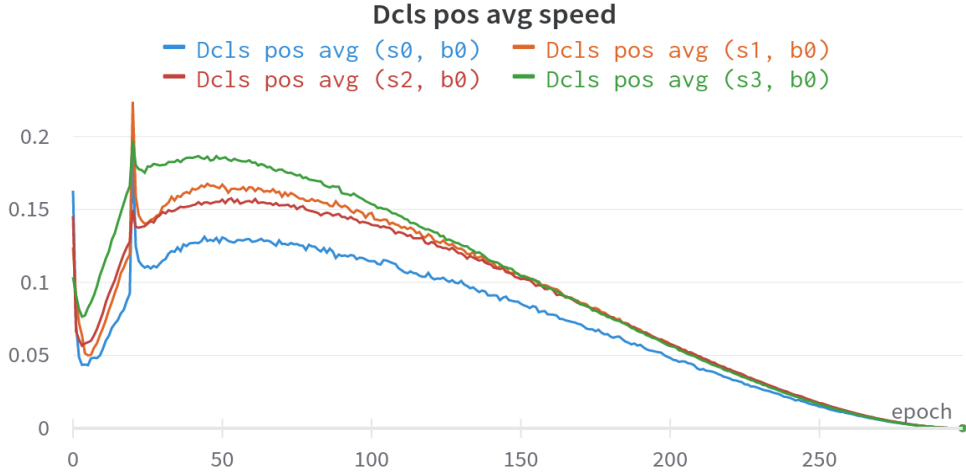


Figure 7: The average speed of the four position tensors for the ConvNeXt-T-dcls model as function of epochs.

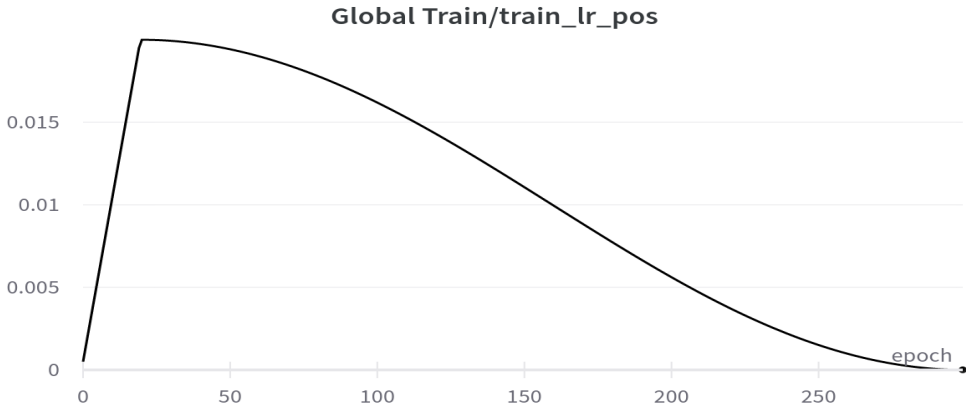


Figure 8: The learning schedule used for training ConvNeXt-T-dcls model.

At epoch 0, we can notice that the average speed is abnormally high, this is due to the fact that in the beginning, the positions are initialized randomly and we arbitrarily considered that $V_{\mathbf{p}}(0) = 0$, thus the large speed gap at initialization. Another peak can be seen at epoch 20, this one is due to the introduction of the repulsive loss (Thomas et al., 2019) at this precise epoch during training. This last causes a momentary increase in the average speed of the DCLS positions. In general, we can say that over epochs, the average DCLS positions follow the shape of the scheduler used in training.

F APPENDIX: EFFECTIVE RECEPTIVE FIELDS COMPARISON

In the following, we show the effective receptive fields (ERF) calculated respectively for ConvNeXt-T-dcls, ConvNeXt-T with standard dilated kernel of rate 2 and ConvNeXt-T models. The input crops used here are of size 1024×1024 and the heatmaps are normalized (between 0 and 1). We observe that the ERF of ConvNeXt-T-dcls is larger than the one of the baseline. It has also a particular shape that resembles a square with more prominent diagonals and medians. The ERF of ConvNeXt-T with a standard dilated kernel is even larger but with gridding artifacts. In all plots, it seems that the center has more importance.

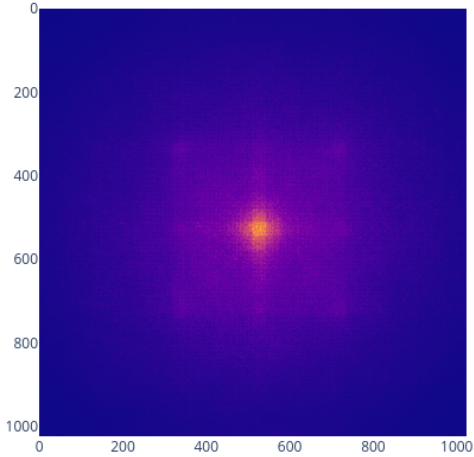


Figure 9: The effective receptive field (ERF) of the ConvNeXt-T-dcls model.

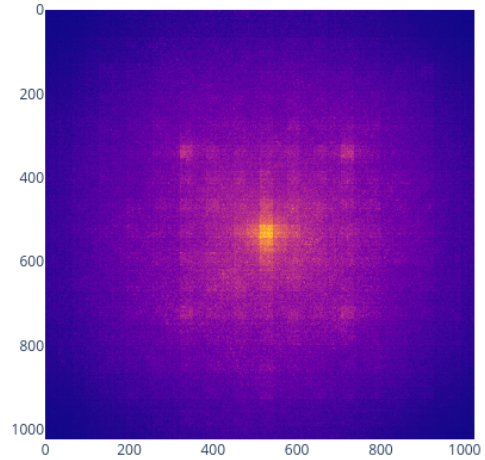


Figure 10: The effective receptive field of the ConvNeXt model with dilated kernels (dilate rate 2) instead of the dense 7×7 ones.

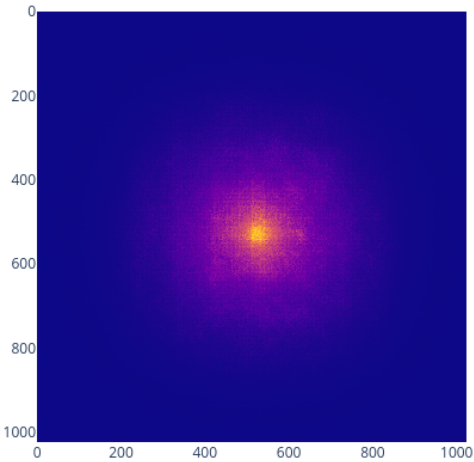


Figure 11: The effective receptive field of the ConvNeXt-T model.